Infrared spectroscopy of Cr- and V-doped Sb_2Te_3: Dilute magnetic semiconductors

J. Manson, A. Madubuonu, and D. A. Crandles*
Department of Physics, Brock University, St. Catharines, Ontario, Canada L2S 3A1

C. Uher
Department of Physics, University of Michigan, Ann Arbor, Michigan 48109, USA

Petr Loš'ták
Department of General and Inorganic Chemistry, Faculty of Chemical Technology, University of Pardubice, Čs. Legií, 565, 532 10 Pardubice, Czech Republic

(Received 5 August 2014; revised manuscript received 20 October 2014; published 6 November 2014)

Temperature dependent optical reflectance measurements on well characterized samples of nonintentionally doped, Cr-doped, and V-doped Sb_2Te_3 show that both the parent compound and the Cr-doped version are narrow-gap semiconductors ($E_g \approx 0.25$ eV) with a conventional Drude free carrier absorption. The carrier density increases slightly with decreasing temperature while the scattering rate increases quadratically with temperature, which is a sign of the importance of optical phonon scattering. Vanadium doping introduces a change in the temperature dependence of the scattering rate as well as higher electrical resistivity than Cr-doped Sb_2Te_3. An analysis of the literature values of the saturation magnetization of $Sb_{2-x}V_xTe_3$ for $H \parallel c$ suggests V is in a mixed valence state V^{3+}/V^{4+}.

DOI: 10.1103/PhysRevB.90.205205 PACS number(s): 75.50.Pp, 78.20.Ci, 78.30.−j

I. INTRODUCTION

Antimony telluride is a member of the $A_2^{\mathrm{V}}B_3^{\mathrm{VI}}$ tetradymite family (A = Sb,Bi; B = Se,Te) of layered narrow-gap semiconductors ($E_g \approx 0.25$ eV [1]). It crystallizes with rhombohedral symmetry in an atomic arrangement most clearly described in terms of layers with a repeating sequence of Te_1-Sb-Te_2-Sb-Te_1 atoms along the c axis [2]. Bonding between Te_1 and Sb atoms is predominantly ionic, while bonding between Te_2 and Sb atoms is mainly covalent. Neighboring layers are weakly held together by van der Waals bonds between Te_1-Te_1 sheets. There has been considerable interest in Sb_2Te_3 in the past decade for at least three reasons: because it is an important thermoelectric material [3], because it is member of a family of topological insulators [4,5], and because it is a dilute magnetic semiconductor (DMS) upon doping with V, Cr, or Fe [6–13]. This work focuses on Sb_2Te_3 as the parent compound of a number of DMS materials.

Following the success of metallic spintronic effects such as giant magnetoresistance, intensive research efforts have been devoted to investigating prospective materials for semiconductor spintronic devices. The most extensively studied materials of this type are II-VI and III-V semiconductors doped with small concentrations (≈1%) of Mn atoms [14,15]. These DMS form in zinc-blende and wurtzite structures with relatively large band gaps, where tetrahedrally bonded Mn^{2+} atoms are responsible for their magnetic properties. In contrast, Sb_2Te_3 is a narrow-gap material in which octahedrally bonded transition metal (TM) impurities coupled by free holes are responsible for the magnetic properties. Specifically, single crystals of $Sb_{1.94}Cr_{0.06}Te_3$ and $Sb_{1.97}V_{0.03}Te_3$ have demonstrated ferromagnetic transition temperatures of $T_c \approx 17$ K and $T_c \approx 22$ K, respectively [6,7]. Low temperature molecular beam epitaxy enables increased TM ion density, and thin films of $Sb_{1.41}Cr_{0.59}Te_3$ and $Sb_{1.65}V_{0.35}Te_3$ have reported Curie temperatures of 190 and 177 K, respectively [8,10]. These materials give one an opportunity to further the understanding of DMS behavior in a completely different setting.

There have been many studies of the optical properties of the $A_2^{\mathrm{V}}B_3^{\mathrm{VI}}$ semiconductors. The earliest optical studies dealt with band structure and transverse optical phonons [16,17]. More recent optical work has focused on studying the more insulating members of the family to find signatures of topological insulator behavior [18–24]. The material of interest in this paper, Sb_2Te_3, is not a good candidate in which to observe these effects since it tends to crystallize in a nonstoichiometric Sb-rich fashion, resulting in a relatively high free hole concentration ($\approx 10^{20}$ cm^{-3}) [6,7,25]. Consequently, Sb_2Te_3 has been observed to have the highest plasma frequency in the family [26]. Optical techniques have proven to play an integral part in determining the role of disorder, band structure, and carrier dynamics in Mn-doped III-V materials [15]. In contrast to the Mn-doped III-V materials where Mn doping introduces both free carriers and TM ions, the localized impurity spins in Sb_2Te_3 are coupled by a preexisting hole gas. The infrared and magnetic results to be discussed below allow one to separate charge density and scattering effects and give insight into the relative importance of different scattering effects in this family of materials.

II. SAMPLES

Samples were cut from single crystal boules that were grown using the modified Bridgman method [27]. Three samples were chosen: one cut from a boule free of either V or Cr, labeled Sb_2Te_3, one from a V-doped boule labeled SVT, and one from a Cr-doped boule labeled SCT. Since the TM ion concentration varies with position along the length of the boules, energy dispersive spectroscopy (EDS) was

*dcrandles@brocku.ca

TABLE I. Sample composition using energy dispersive spectroscopy data.

Label	Composition	Sb (±0.1 at. %)	Te (±0.1 at. %)	V (±0.1 at. %)	Cr (±0.1 at. %)	x	y
Sb_2Te_3	$Sb_{2+y}Te_{3-y}$	41.2	58.8	0	0	0	0.06
SCT	$Sb_{2+y-x}Cr_xTe_{3-y}$	39.3	59.1	0	1.6	0.08	0.045
SVT	$Sb_{2+y-x}V_xTe_{3-y}$	40.1	58.8	1.1	0	0.055	0.06

used to determine the precise stoichiometry of the samples (JEOL JSM-7000F). As shown in Table I, the sample labeled Sb_2Te_3 is actually slightly Sb rich, which is common in this family of materials. This results in Te vacancies and/or antisite defects, where out of the six possible locations for Sb substitution for Te, excess Sb resides predominately in Te_1 sites [28]. The excess antimony provides free holes, resulting in a highly degenerate *p*-type semiconductor. For comparison with previous work, which has not explicitly considered excess Sb when referring to sample composition, SVT and SCT might have been labeled $Sb_{1.945}V_{.055}Te_3$ and $Sb_{1.92}Cr_{.08}Te_3$, respectively.

The temperature dependence of the dc electrical resistivity measured using the van der Pauw technique appears in Fig. 1. The data show the same features as previous measurements taken on samples with a similar level of V or Cr concentration [6,7]. Note that sample SVT has a higher electrical resistivity than sample SCT despite having a lower TM ion concentration. Note also the features near 20 K in samples SVT and SCT, which indicate the onset of the ferromagnetic transitions in these samples. Further evidence of the ferromagnetic transition in these samples appears in Fig. 2, which illustrates the magnetic hysteresis data taken with a quantum design magnetic property measurement system (MPMS). Note that the measured saturation magnetization for sample SCT is higher than expected for Cr^{3+} (it should be 2.2 emu/g for the Cr concentration measured in Table I) while the saturation magnetization of SVT is less than that expected for V^{3+} (it should be 1.1 emu/g for the V concentration measured in Table I), as will be discussed in more detail below. In agreement with previous work, the coercive field of the SCT sample is lower than that of the SVT sample, and the Cr-doped sample becomes magnetically fully saturated at a lower field [7].

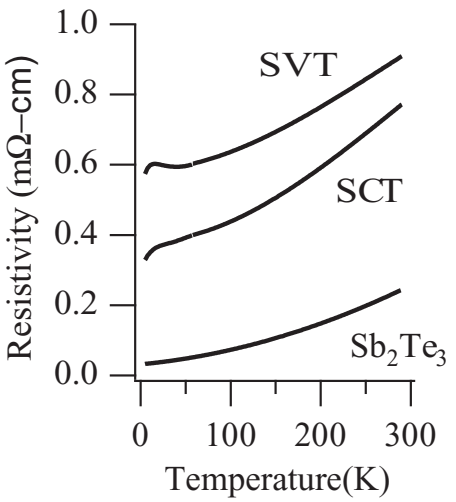

FIG. 1. Resistivity vs temperature of samples Sb_2Te_3, SVT, and SCT. See Table I for composition.

III. RESULTS AND DISCUSSION

Measurements of normal incidence absolute reflectance spectra were collected at many temperatures using unpolarized light with the electric field perpendicular to the *c* axis on freshly cleaved mirror-quality surfaces (area ≈ 0.5 cm^2). The data were collected with use of a Bruker IFS 66/V spectrometer from 50 to 10 000 cm^{-1}, with temperature control provided by a Janis cryostat that allowed for measurements from 20 to 300 K [29], and normalized via *in situ* gold evaporation [30]. Some of the reflectance spectra collected appear in Fig. 3. Data at many more temperatures were collected, but Fig. 3 illustrates the most important trends. Note the plasma edge between 1000 and 1500 cm^{-1} that can be seen to move to higher energy and deepen with decreasing temperature in all three samples. The increase of plasma frequency with decreasing temperature has also been observed in Bi_2Te_3 [26,31] but not in Bi_2Se_3 [19,26]. Note that the plasma edge occurs at about the same frequency in Sb_2Te_3, SCT, and SVT, indicating a similar free carrier density in all three samples at room temperature,

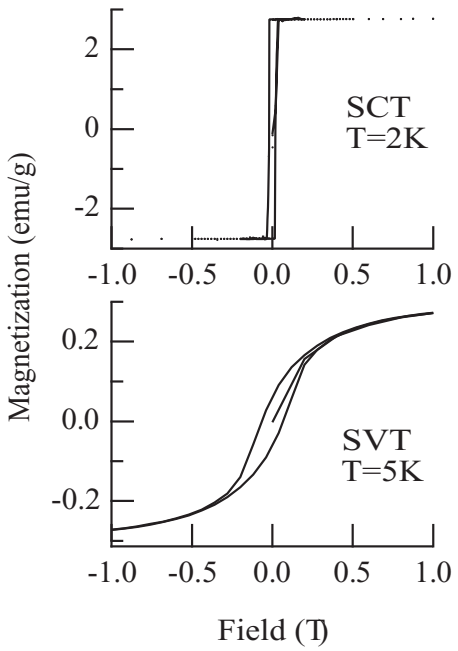

FIG. 2. Magnetization vs field of samples SVT and SCT. See Table I for composition.

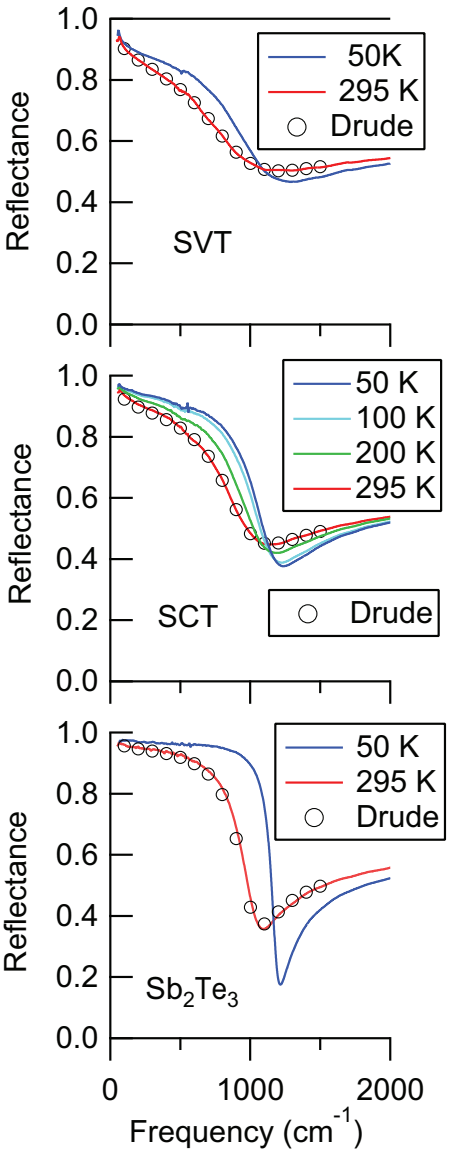

FIG. 3. (Color online) Reflectance spectra at various temperatures for samples of Sb_2Te_3, SVT, and SCT. Fits to the Drude model for the 295 K (open circles) are also shown.

which is consistent with the Hall data, to be discussed below. The depth of the reflectance minimum just above the plasma edge varies inversely with the scattering rate, implying the lowest scattering for the undoped sample Sb_2Te_3, which is expected. Reflectance data were also collected on a second sample from the V-doped boule, labeled SVT2, and cleaved perpendicular to the c axis but 0.5 mm further down the axis of the boule. Figure 4 presents reflectance spectra collected on sample SVT2 above and below the Curie temperature, which indicates that there is no significant change in plasma frequency accompanying the ferromagnetic transition [29].

The optical data were first analyzed by fitting the normal incidence reflectance spectra between 100 and 1500 cm^{-1} to the appropriate Fresnel equation using the Drude model [32] for the complex dielectric function $\tilde{\epsilon} = \epsilon_\infty - \frac{\omega_p^2}{(\omega^2 - i\omega\Gamma)}$. In this equation ω is the frequency of the incident light, Γ is the

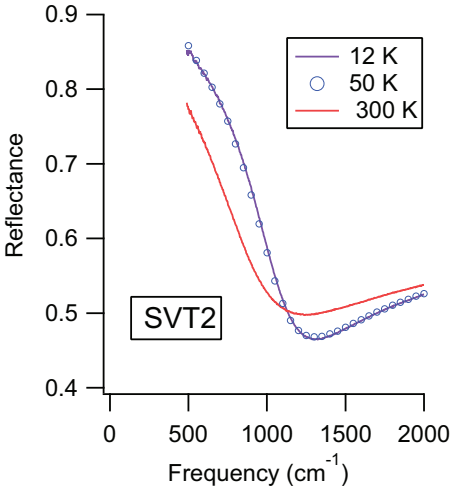

FIG. 4. (Color online) Reflectance of sample SVT2 at temperatures above (50 and 300 K) and below (12 K) the ferromagnetic transition.

scattering rate, and the plasma frequency ω_p is related to the free carrier concentration N and effective mass of the carriers m^* via the equation $\omega_p^2 = \frac{4\pi Ne^2}{m^*}$. Sample fits are shown in Fig. 3. The plasma frequencies determined in the fits are shown in Fig. 5. Shown in the same graph are independent measurements of free hole concentrations determined from Hall data assuming a single band. The Hall coefficient versus temperature was measured using a Quantum Design physical property measurement system (PPMS) with use of the ac

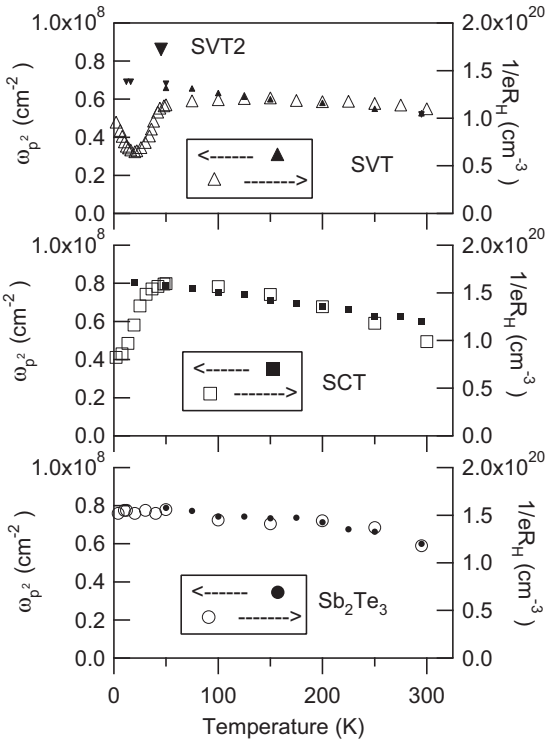

FIG. 5. Square of plasma frequency obtained in the fits to the reflectance data and hole concentration determined from Hall measurements ($p = 1/eR_H$) vs temperature.

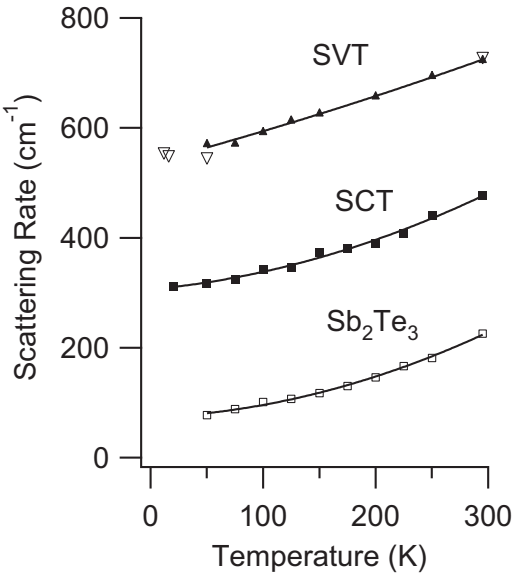

FIG. 6. Scattering rates obtained in fits of the reflectance data vs temperature. Open squares: Sb_2Te_3. Solid squares: SCT. Solid triangles are from fits to reflectance data collected on sample SVT, some of which are shown in Fig. 3. Open triangles are from fits to reflectance spectra of sample SVT2, whose representative curves are shown in Fig. 4. Solid lines are fits to $\Gamma = a + bT + cT^2$.

transport option at 16 Hz in the presence of a half tesla field. Note the increase in carrier density with decreasing temperature. This is consistent with observations of an increase in plasma frequency with decreasing temperature in other heavily doped semiconductors and metals [33–35]. While R_H is approximately constant below 50 K for sample Sb_2Te_3, there is an increase in R_H at low temperature in the data for samples SVT and SCT which is associated with the onset of the ferromagnetic transition and is consistent with previous measurements [6,7]. The combined plasma frequency and carrier density measurements illustrated in Fig. 5 suggest a temperature independent effective mass of approximately $m^* = 0.18m_e$, which is comparable to that determined for Bi_2Te_3 [31].

The scattering rates determined via the reflectance fits are plotted in Fig. 6. The metallic resistivity behavior illustrated in Fig. 1 is thus conventionally metallic: relatively constant free carrier density and a scattering rate that increases with temperature. The $\Gamma(T)$ curves do not appear linear and so the scattering rate must be governed by more than acoustic phonon scattering. Simple fits of the scattering rate versus temperature ($\Gamma = a + bT + cT^2$) were performed with the fitting parameters presented in Table II. The increase in the

TABLE II. Least square fitting parameters to polynomial fit to scattering rate: $\Gamma = a + bT + cT^2$.

Sample	Fitting range (K)	a (cm^{-1})	b (cm^{-1}/K)	c (cm^{-1}/K^2)
Sb_2Te_3	50–300	73 ± 5	0.08 ± 0.06	0.0014 ± 0.0002
SCT	20–300	306 ± 6	0.19 ± 0.08	0.0013 ± 0.0003
SVT	50–300	536 ± 8	0.55 ± 0.11	0.0003 ± 0.0003

temperature independent term a when comparing SCT and SVT with Sb_2Te_3 can be explained by the additional presence of magnetic scattering from the Cr^{3+} or V^{3+} impurities. Note that the largest term at 300 K in Sb_2Te_3 is the T^2 contribution. A T^2 temperature dependence at extremely low temperatures is evidence of electron-electron scattering, but at higher temperatures may be an indication of the importance of optical in addition to acoustic phonon scattering. A superlinear dependence of resistivity on temperature has been observed in certain metal oxides and has been attributed to optical phonon scattering [36,37]. It is interesting to note that in our sample of Sb_2Te_3, if one excludes the temperature independent contribution ($a = 73 \pm 5$ cm^{-1}), the room temperature scattering rate (223 ± 5 cm^{-1}) is about the same as that measured in $Bi_{2.002}Te_{2.998}$ (22 meV or 177 cm^{-1} at 300 K) [31]. Thomas *et al.* suggested that the very small value of the temperature independent contribution to scattering observed in $Bi_{2.002}Te_{2.998}$ is due to substitution of excess Bi in Te^1 sites, which affects the density of states only at energies far from the Fermi level. The larger value of static impurity scattering in our sample of Sb_2Te_3 can be explained by the fact that the amount of excess Sb is ten times the amount of excess Bi in the sample that Thomas *et al.* studied [31]. The excess Sb is accompanied by Te vacancies as well as antisite defects.

Note that the temperature dependent terms (b,c) are essentially the same within experimental error for Sb_2Te_3 and SCT but different for SVT. This is an indication that the dominant mechanisms governing scattering are different in SVT. In addition, the resistivity approaches 1 mΩ cm, making SVT similar in behavior to "bad metals" such as the high T_c superconductors and $SrRuO_3$ [38,39]. An explanation for the vanadium induced changes in the scattering rate might come from measurements of the saturation magnetization in $Sb_{2-x}Cr_xTe_3$ and $Sb_{2-x}V_xTe_3$. Recall that our measurements indicated that the measured saturation magnetization of our SCT sample was greater than expected, but that of SVT was less than expected. A smaller than expected saturation magnetization in $Sb_{1.97}V_{0.03}Te_3$ is also seen in Fig. 6 of Ref. [7]. We decided to reexamine all the existing literature data of magnetic saturation measurements with the field parallel to the c axis. The data are presented in Fig. 7. Note that the literature values for $Sb_{2-x}Cr_xTe_3$ are consistent with $S = 3/2$ or Cr^{3+} ions for all Cr concentrations in thin films and in crystals. On the other hand, the data for $Sb_{2-x}V_xTe_3$ are not so clear cut, suggesting $S = 1/2$ in some samples of SVT. The data thus suggest a mixed valence state for vanadium (V^{3+}/V^{4+}). It is this "Coulomb disorder" that could be the source of the different temperature dependences of scattering rate in SVT and SCT. Unfortunately the vanadium concentration in our sample of SVT precludes accurate x-ray photoelectron spectroscopy measurements that might confirm the mixed valence state of vanadium.

To gain some insight into the different scattering mechanisms in SVT, it is instructive to look at the real optical conductivity obtained by a Kramers-Kronig analysis (KK) of the reflectance data, which is shown in Figs. 8 and 9. Conventional high and low frequency extrapolations (Hagens-Rubens) were used for the reflectance in the KK calculation. Figure 8 shows the free carrier absorption peak centered at 0 cm^{-1} and the onset of interband absorption above

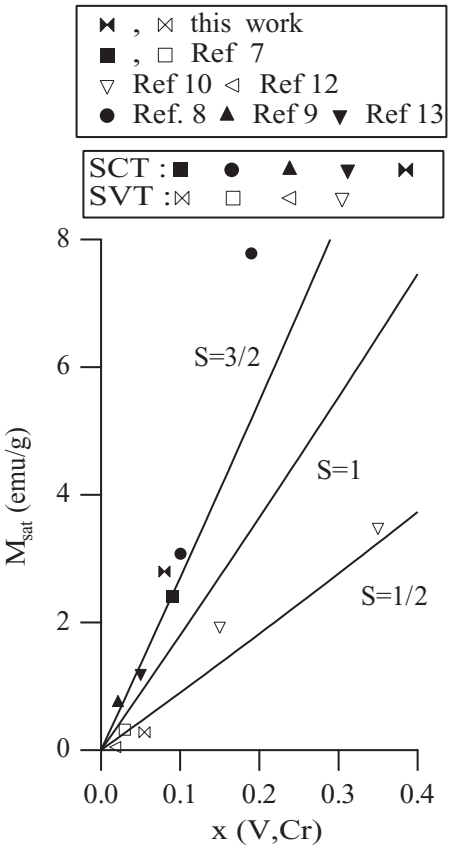

FIG. 7. Literature values of the low temperature saturation magnetization in $Sb_{2-x}Cr_xTe_3$ and $Sb_{2-x}V_xTe_3$ systems for both crystals ($x < 0.09$) and thin films ($x > 0.09$) compared with the expected values for $S = 3/2$, $S = 1$, and $S = 1/2$ ions.

approximately 2000 cm^{-1}. The spectrum is exactly what is expected for a narrow-gap semiconductor at high temperature when the electron gas becomes degenerate. Because the band gap is so small, the absorption does not fall to zero between the free carrier absorption peak and the interband absorption. The upper panel of Fig. 9 compares the KK real conductivity of Sb_2Te_3 with that calculated using the Drude model using parameters obtained in the fit to the reflectance data shown

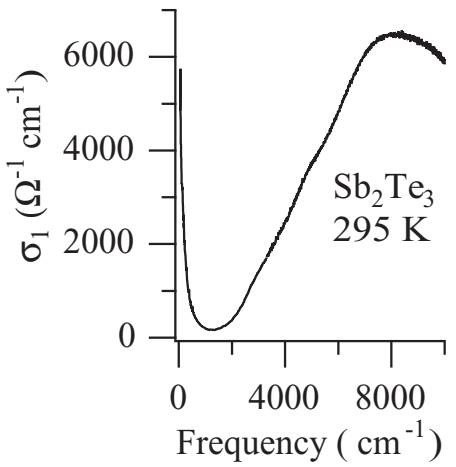

FIG. 8. Optical conductivity of Sb_2Te_3 at room temperature.

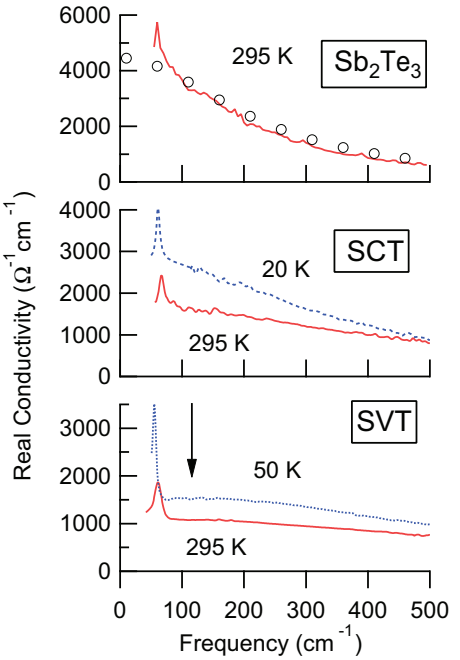

FIG. 9. (Color online) Optical conductivity at various temperatures (solid and dashed lines) of Sb_2Te_3, SCT, and SVT obtained via a Kramers-Kronig analysis of the reflectance data. The open circles in the upper panel show the real optical conductivity calculated using the Drude model for the dielectric function with plasma frequency $\omega_p = 7730$ cm^{-1} and scattering rate $\Gamma = 223$ cm^{-1}, parameters that were found when making fits to the reflectance data in Fig. 3.

in Fig. 3. The relatively good agreement between the KK conductivity and the Drude model conductivity indicates the free carrier response of the parent material Sb_2Te_3 is completely conventional. The peak observed near 69 cm^{-1} in the upper panel of Fig. 9 is due to absorption by the transverse optical phonon, which has been observed by earlier workers [17]. This phonon softens by roughly 5–6 cm^{-1} as the temperature is lowered to 50 K. The lower two panels of Fig. 9 compare the real conductivity of SCT and SVT at 295 K and a

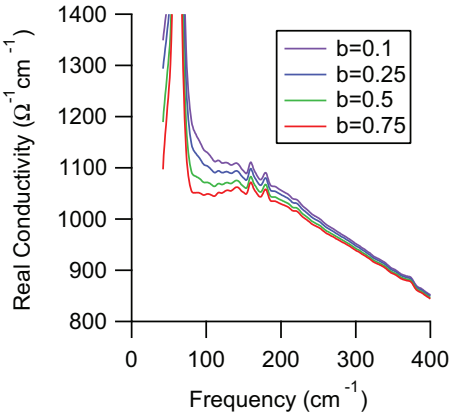

FIG. 10. (Color online) Optical conductivity of SVT at 295 K obtained via a Kramers-Kronig analysis of the reflectance data. The curves were generated using different low frequency extrapolations $R = 1 - a\omega^b$, where $b = 0.5$ is the usual Hagens-Rubens extrapolation.

lower temperature. A potentially interesting feature in the SVT data is indicated by the arrow. At these frequencies (roughly between 100 and 130 cm^{-1}), the slope $\frac{d\sigma_1}{d\omega} > 0$ if one uses a Hagens-Rubens-like extrapolation for $\omega < 50\,cm^{-1}$. However, the slope proves to be sensitive to the actual extrapolation used as seen in Fig. 10 and remains an open question. If it does turn out to be positive, this non-Drude-like response could have several interpretations, including a Fano-type coupling of the phonon to the hole gas, an impurity absorption that overlaps with the free carrier absorption or, perhaps, a degree of weak localization associated with disorder [40–42], which is consistent with a mixed valence state for vanadium.

IV. CONCLUSIONS

Temperature dependent optical reflectance measurements on well characterized samples of nonintentionally doped, Cr-doped, and V-doped Sb_2Te_3 show that both the parent compound and the Cr-doped version are narrow-gap semiconductors ($E_g \approx 0.25$ eV) with a conventional Drude free carrier absorption. The carrier density increases slightly with decreasing temperature while the scattering rate increases quadratically with temperature, which is a sign of the importance of optical phonon scattering. Vanadium doping introduces a change in the temperature dependence of the scattering rate as well as higher electrical resistivity than in Cr-doped Sb_2Te_3. An analysis of the literature values of the saturation magnetization of $Sb_{2-x}V_xTe_3$ for $H \parallel c$ suggests V is in a mixed valence state V^{3+}/V^{4+}.

ACKNOWLEDGMENTS

Financial support for this work was provided by the Natural Sciences and Engineering Research Council of Canada. We acknowledge discussions with S. K. Bose and the use of F. Razavi's superconducting quantum interference device (SQUID) magnetometer and PPMS systems, which were funded by the Canadian Foundation for Innovation and the Ontario Research Fund. C. Butcher of the Canadian Center for Electron Microscopy at McMaster University made the EDS measurements. We especially thank J. Hall of T. Timusk's laboratory for the SVT reflectance data below 20 K.

[1] R. Rönnlund, O. Beckmann, and H. Levy, J. Phys. Chem. Solids **26**, 1281 (1965).
[2] P. Larson, Phys. Rev. B **74**, 205113 (2006).
[3] G. Wang and T. Cagin, Phys. Rev. B **76**, 075201 (2007).
[4] D. Hsieh, Y. Xia, D. Qian, L. Wray, F. Meier, J. H. Dil, J. Osterwalder, L. Patthey, A. V. Fedorov, H. Lin, A. Bansil, D. Grauer, Y. S. Hor, R. J. Cava, and M. Z. Hasan, Phys. Rev. Lett. **103**, 146401 (2009).
[5] H. Ke, M. Xu-Cun, C. Xi, L. Li, W. Ya-Yu, and X. Qi-Kun, Chin. Phys. B **22**, 067305 (2013).
[6] J. S. Dyck, P. Hájek, P. Lošt'ák, and C. Uher, Phys. Rev. B **65**, 115212 (2002).
[7] J. S. Dyck, Č. Drašar, P. Lošt'ák, and C. Uher, Phys. Rev. B. **71**, 115214 (2005).
[8] Z. Zhou, Y.-J. Chien, and C. Uher, Appl. Phys. Lett. **87**, 112503 (2005).
[9] V. A. Kulbachinskii, P. M. Tarasov, and E. Brük, JETP Lett. **81**, 342 (2005).
[10] Z. Zhou, Y.-J. Chien, and C. Uher, Phys. Rev. B **74**, 224418 (2006).
[11] Z. Zhou, M. Žabčík, P. Lošt'ák, and C. Uher, J. Appl. Phys. **99**, 043901 (2006).
[12] Z. Zhou, C. Uher, M. Žabčík, and P. Lošt'ák, Appl. Phys. Lett. **88**, 192502 (2006).
[13] H. Li, Y. R. Song, M.-Y. Yao, F. Yang, L. Miao, F. Zhu, C. Liu, C. L. Gao, D. Qian, X. Yao, J.-F. Jia, Y. J. Shi, and D. Wu, Appl. Phys. Lett. **101**, 072406 (2012).
[14] D. Ferrand, C. Bourgognon, J. Cibert, A. Wasiela, S. Tatarenko, Y. Merle d'Aubigné, A. Bonnani, D. Stifter, H. Sitter, Le Van Khoi, S. Koleśnik, J. Jaroszyński, M. Sawicki, T. Andrearczyk, and T. Dietl, Physica B **284-288**, 1177 (2000).
[15] K. S. Burch, D. D. Awshalom, and D. N. Basov, J. Magn. Magn. Mater. **320**, 3207 (2008).
[16] D. L. Greenaway and G. Harbeke, J. Phys. Chem. Solids **26**, 1585 (1965).
[17] W. Richter, H. Köhler, and C. R. Becker, Phys. Status Solidi B **84**, 619 (1977).
[18] N. P. Butch, K. Kirshenbaum, P. Syers, A. B. Sushkov, G. S. Jenkins, H. D. Drew, and J. Paglione, Phys. Rev. B **81**, 241301 (2010).
[19] A. D. LaForge, A. Frenzel, B. C. Pursley, T. Lin, X. Liu, J. Shi, and D. N. Basov, Phys. Rev. B **81**, 125120 (2010).
[20] P. Di Pietro, F. M. Vitucci, D. Nicoletti, L. Baldassarre, P. Calvani, R. Cava, Y. S. Hor, U. Schade, and S. Lupi, Phys. Rev. B **86**, 045439 (2012).
[21] R. Valdés Aguilar, A. V. Stier, W. Liu, L. S. Bilbro, D. K. George, N. Bansal, L. Wu, J. Cerne, A. G. Markelz, S. Oh, and N. P. Armitage, Phys. Rev. Lett. **108**, 087403 (2012).
[22] Liang Wu, M. Brahlek, R. Valdés Aguilar, A. V. Stier, C. M. Morris, Y. Lubashevsky, L. S. Bilbro, N. Bansal, S. Oh, and N. P. Armitage, Nat. Phys. **9**, 410 (2013).
[23] K. W. Post, B. C. Chapler, L. He, X. Kou, K. L. Wang, and D. N. Basov, Phys. Rev. B **88**, 075121 (2013).
[24] A. A. Reijnders, Y. Tian, L. J. Sandilands, G. Pohl, I. D. Kivlichan, S. Y. F. Zhao, S. Jia, M. E. Charles, R. J. Cava, N. Alidoust, S. Xu, M. Neupane, M. Z. Hasan, X. Wang, S. W. Cheong, and K. S. Burch, Phys. Rev. B **89**, 075138 (2014).
[25] J. Horák, P. C. Quayle, J. S. Dyck, Č. Drašar, P. Lošt'ák, and C. Uher, J. Appl. Phys. **103**, 013516 (2008).
[26] S. V. Dordevic, M. S. Wolf, N. Stojilovic, H. Lei, and C. Petrovic, J. Phys.: Condens. Matter **25**, 075501 (2013).
[27] P. Lošt'ák, Č. Drašar, J. Navrátil, and L. Beneš, Cryst. Res. Technol. **31**, 403 (1996).
[28] T. Thonhauser, G. S. Jeon, G. D. Mahan, and J. O. Sofo, Phys. Rev. B **68**, 205207 (2003).
[29] The subset of data on sample SVT2 was taken by J. Hall in T. Timusk's laboratory at McMaster University in order to reach below 20 K.
[30] C. C. Homes, T. Timusk, M. Reedyk, and D. A. Crandles, Appl. Opt. **32**, 2976 (1993).

[31] G. A. Thomas, D. H. Rapkine, R. B. Van Dover, L. F. Mattheiss, W. A. Sunder, L. F. Schneemeyer, and J. V. Waszczak, Phys. Rev. B **46**, 1553 (1992).
[32] M. Dressel and G. Grüner, *Electrodynamics of Solids* (Cambridge University Press, Cambridge, UK, 2002).
[33] M. Ortolani, P. Calvani, and S. Lupi, Phys. Rev. Lett. **94**, 067002 (2005).
[34] F. Carbone, A. B. Kuzmenko, H. J. A. Molegraaf, E. van Heumen, E. Giannini, and D. van der Marel, Phys. Rev. B **74**, 024502 (2006),
[35] A. A. Reijnders, J. Hamilton, V. Britto, J.-B. Brubach, P. Roy, Q. D. Gibson, R. J. Cava, and K. S. Burch, arXiv:1408.0008v1.
[36] W. D. Ryden, A. W. Lawson, and C. C. Sartain, Phys. Lett. A **26**, 209 (1968).
[37] C. N. King, H. C. Kirsch, and T. H. Geballe, Solid State Commun. **9**, 907 (1971).
[38] V. J. Emery and S. A. Kivelson, Phys. Rev. Lett. **74**, 3253 (1995).
[39] L. Klein, J. S. Dodge, C. H. Ahn, J. W. Reiner, L. Mieville, T. H. Geballe, M. R. Beasley, and A. Kapitulnik, J. Phys.: Condens. Matter **8**, 10111 (1996).
[40] P. Kostic, Y. Okada, N. C. Collins, Z. Schlesinger, J. W. Reiner, L. Klein, A. Kapitulnik, T. H. Geballe, and M. R. Beasley, Phys. Rev. Lett. **81**, 2498 (1998).
[41] D. A. Crandles, B. Nicholas, C. Dreher, C. C. Homes, A. W. McConnell, B. P. Clayman, W. H. Gong, and J. E. Greedan, Phys. Rev. B **59**, 12842 (1999).
[42] D. A. Crandles, M. M. Yazdanian, and F. S. Razavi, J. Phys. D: Appl. Phys. **39**, 6 (2006).